Supporting Information

Ultralight, elastic carbon nanofiber aerogel for efficient energy storage and sorption properties

Xing Jin, Ahmed Al-Qatatsheh, Karamat Subhani, Nisa V Salim

Faculty of Science, Engineering and Technology, Swinburne University of Technology, Hawthorn 3122, Victoria, Australia

S1 Normalization of the saturated sorption capacities of various oils and organic solvents by their density

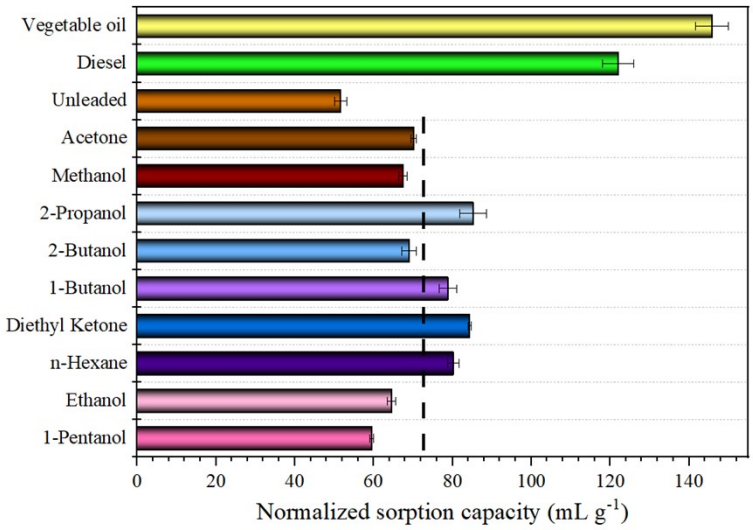

S2 Modelling of G/CNF foam

S2.1 Graphene Coating Microstructure

Graphene coating microstructure was calculated and characterized using the approach we reported previously [1].

S2.2 Constitutive Models

A homogenization strategy is needed to derive the useful parameters of the material points of a continuum to predict G/CNFs morphology and electrical properties. We utilized experimental outcomes to characterize the microstructure of the different phases within the structured matrix. Then, we ran several geometry scenarios to predict G/CNFs morphology and followed several homogenization strategies to predict electrical properties associated with such nanofibers. In our homogenization calculation procedure, we considered the isotropic and the transverse isotropic properties of the CNFs and the Graphene coating. While the electric conductivity of the CNFs was 150.0 S/m, the electrical conductivity of the Graphene coating was 1738 S/m [2, 3]. The air in the air-filled porous microstructure (i.e., 99.0 %) was considered an isotropic dielectric material with an electrical conductivity of 1.0×10^{-8} S/m [4].

S2.3 Homogenization Models

The electrical conductivity tensor of G/CNFs has been modeled using several models, covering Elshelby Model [5, 6], Mori-Tanaka (M-T) model [7], and Maxwell [8]. Here, we have utilized the MFH model based on the D-I model using the Multi-level method as implemented in Digimat-MF [9]. We chose the MFH model because it does not require an RVE generation and meshing. Likewise, we decided on the multi-level method based on the Nested Homogenization Level because it provides fast, accurate, and efficient prediction at the microscopic level when implementing coated inclusion. Table S2-1 summarises the experimental and referenced data utilized in the homogenization. Also, we considered that both Graphene and CNFs are perfectly bonded.

Table **S2-1** Summary of experimental and referenced data utilized in microelectrical modeling

S/N	Property	Unit	Value	Remark
1.0	G/CNFs Average Diameter	nm	560.000	• Calculated Value
2.0	Graphene Flakes Average Diameter	nm	50.000	• Estimated Value.
3.0	Graphene Flake Thickness (Range)	nm	0.400–1.000	• Estimated Value.
4.0	Average Graphene Coating	nm	3.2	• Estimated Value.
5.0	CNFs Density	g/cm^3	1.500	• N/A.
6.0	Graphene Density	g/cm^3	2.267	• N/A.
7.0	Porosity	%	99.000	• Calculated Value.
8.0	Average Aspect Ratio	-	$\geq$ 50.000	• Referenced [10]
9.0	G/CNF Volume Fraction	-	0.011	• Calculated Value.

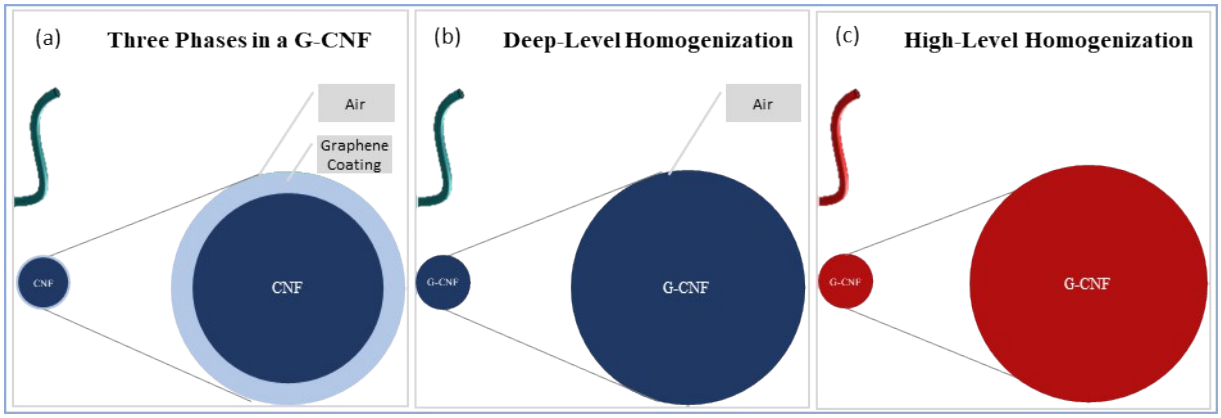

Figure S1 depicts the overall MFH model we used in our modeling, and Figure S2 depects input voltage gradient and its associated current desnisty gradient.

Table S2-1 Summary of experimental and referenced data utilized in microelectrical modeling

S/N	Property	Unit	Value	Remark
1.0	G/CNFs Average Diameter	nm	560.000	• Calculated Value
2.0	Graphene Flakes Average Diameter	nm	50.000	• Estimated Value.
3.0	Graphene Flake Thickness (Range)	nm	0.400–1.000	• Estimated Value.
4.0	Average Graphene Coating	nm	3.2	• Estimated Value.
5.0	CNFs Density	g/cm^3	1.500	• N/A.
6.0	Graphene Density	g/cm^3	2.267	• N/A.

S/N	Property	Unit	Value	Remark
7.0	Porosity	%	99.000	• Calculated Value.
8.0	Average Aspect Ratio	-	≥ 50.000	• Referenced [10]
9.0	G/CNF Volume Fraction	-	0.011	• Calculated Value.

Figure S1 MFH model using the Multi-level method (a) three phases in a G/CNF (b) Deep-Level Homogenization (Graphene – CNF phases), and (c) High-Level Homogenization.

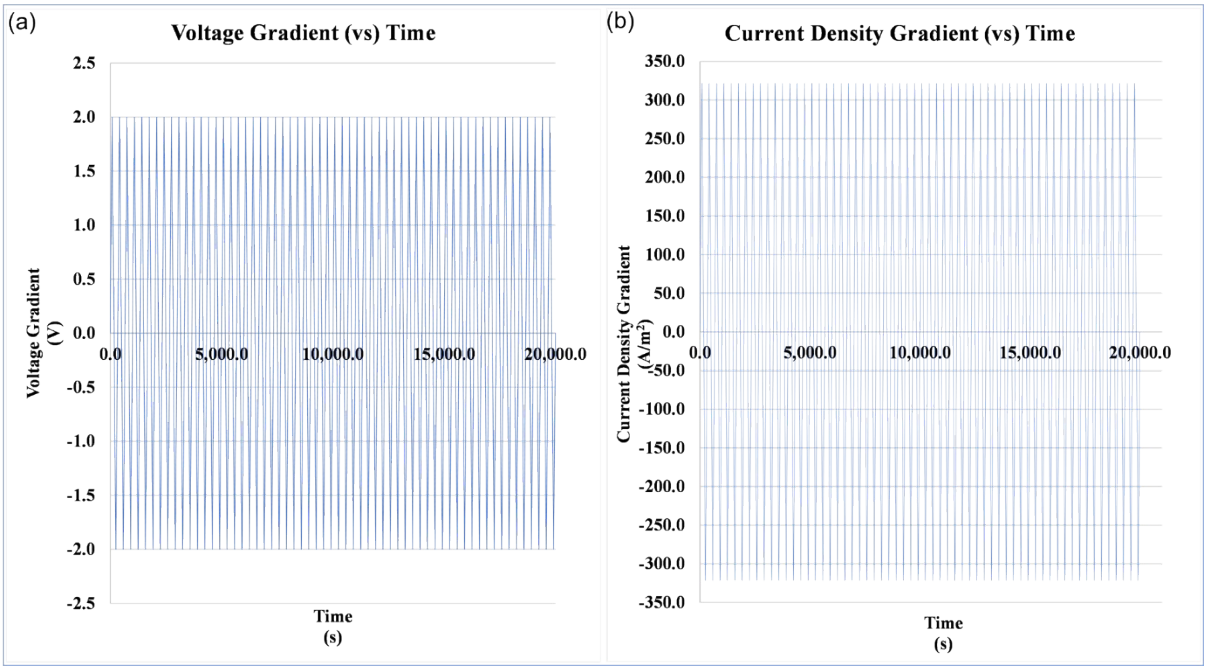

Figure S2 Input (a) voltage gradient (vs) time, and (b) current density (vs) time.

The (D-I) model presumed that each inclusion in each phase (i) is wrapped with a hollow inclusion (i_o) of electrical conductivity C_o, and the outer material has an electrical conductivity C_r. Also, the model presumed that both inclusions have the same aspect ratio, symmetry axis, and center, and their volume ratio equals that of inclusions and matrix in the actual composite. By choosing C_r equals to C_o, the (M-T) model can be retrieved from the (D-I) model, which can be summarised in equations (1-6) [11, 12]:

$$J = \sigma E \quad (1)$$

$$\langle e \rangle = \bar{e}, \langle j \rangle = \bar{j} \ \ with \ \ \langle f \rangle \equiv \frac{1}{V}\int f(\bar{x},x)dV \quad (2)$$

$$\langle f \rangle \equiv V_f^M \langle f \rangle_M + \sum_{i=1}^{N} V_f^i \langle f \rangle_M \quad (3)$$

Where;

J is current density vector, E is the electric field, and σ is the electric conductivity (i.e., $\sigma = \frac{1}{R}$, where R is the electric resistance). The electric conductivity can be

Isotropic, where

$$\sigma = k\begin{bmatrix} 1 & 0 & 0 \\ 0 & 1 & 0 \\ 0 & 0 & 1 \end{bmatrix}$$

Transversally Isotropic, where

$$\sigma = \begin{bmatrix} k_1 & 0 & 0 \\ 0 & k_1 & 0 \\ 0 & 0 & k_1 \end{bmatrix}$$

Or, orthotopic, where

$$\sigma = \begin{bmatrix} k_1 & 0 & 0 \\ 0 & k_2 & 0 \\ 0 & 0 & k_3 \end{bmatrix}$$

$\langle e \rangle$ is the mean-field electric field, and $\langle j \rangle$ is the mean-field current density in each phase (i). f is a macro field, V_f^M is the volume fraction of the matrix phase, and V_f^i is the volume fraction of the inclusion phase.

In a single inclusion phase, if both matrix and inclusion are in an isothermal linear relationship (i.e., Ohm Law), and all inclusions have the same shape, aspect ratio, orientation, and material properties, then the electric field average per phase is related to the electric field average of the matrix through an electric field concentration tensor **B**.

$$\langle e\rangle_i = B{:}\langle e\rangle_M,\ \langle e\rangle_i = A{:}\bar{e} \quad (4)$$

$$A = B{:}(V_f^1 B + V_f^M I)^{-1} \quad (5)$$

$$\bar{C} = \left[V_f^1 C_i{:}B + (1 - V_f^1)C_M\right]{:}\left[V_f^1 B + (1 - V_f^1)I\right]^{-1} \quad (6)$$

Where; $\bar{C}$ is the Macro electrical conductivity.

The results of the implementation of the (D-I) model revealed an improvement of around 8.0 % in the G/CNFs conductivity. This improvement can be due to the effect of Graphene on the CNF conductivity measured in the axial direction when comparing the thickness of Graphene coating to the diameter of CNF, which is only less than 1.0%.

S2.4 G/CNFs Microstructure

The G/CNFs microstructure was stochastically generated as implemented in Digimat-FE. The electrical properties were modeled, and Finite Element Analysis (FEA) was performed using Abaqus/CAE 2020. The G/CNFs foam was represented with two phases; the G/CNFs, which have been previously harmonized as described in section S2.4, and the air. A G/CNF was modeled as a curved cylinder using data in Table S2-1 with relatively high tortuosity (i.e., 8 out of 10) to ensure accurate representation of the modeled material [13]. A 3D RVE model (42.0 μm × 42.0 μm × 42.0 μm) with a total number of 115 inclusions was created and maintained at least 25 times the diameter of the inclusion to ensure statistical significance [14, 15]. G/CNF length was generated randomly using a normal distribution with a mean of 28 μm, and a standard deviation of 2.5 μm. We did not consider the use of specific clustering regions of G/CNFs within the generated RVE as the composite matrix

used in modeling implementation is air, which does support this assumption; furthermore, this was reconfirmed by a careful review of the current SEM does not support such consideration. Although the minimum relative distance between inclusions was maintained to zero, the interpenetration of inclusion was not allowed in our implementation. Also, all phases were generated simultaneously. Figure S3 illustrates a 3D RVE of the generated G/CNFs microstructure with three different views, and Figure S4 provides additional morphological properties of the G/CNFs microstructure.

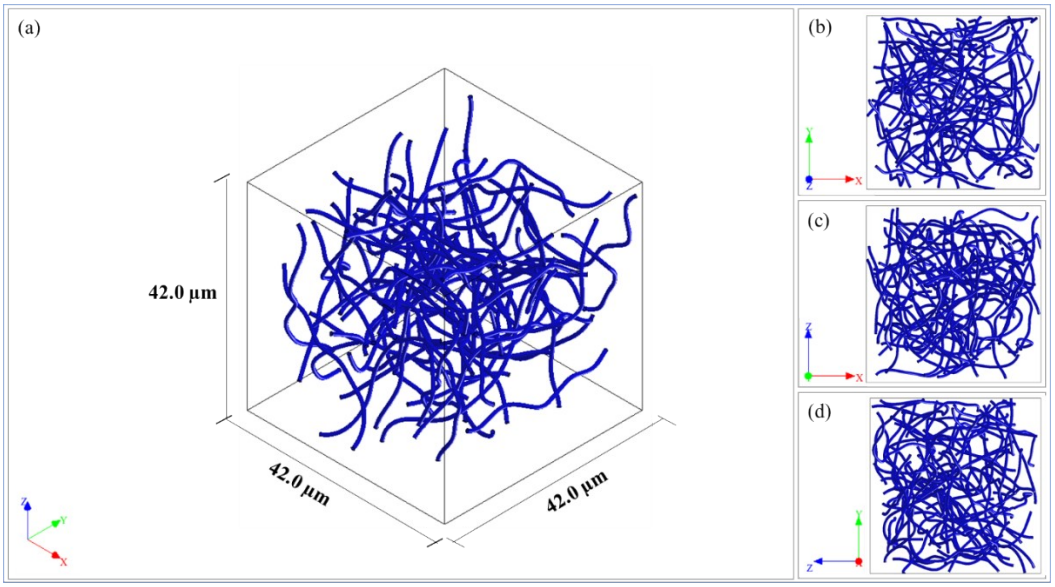

Figure S3 A 3D RVE of G/CNFs Microstructure statistically generated using Digimat-FE, (a) 3D RVE view, (b) X-Y RVE view, (c) X-Z RVE view, and (d) Z-Y RVE view.

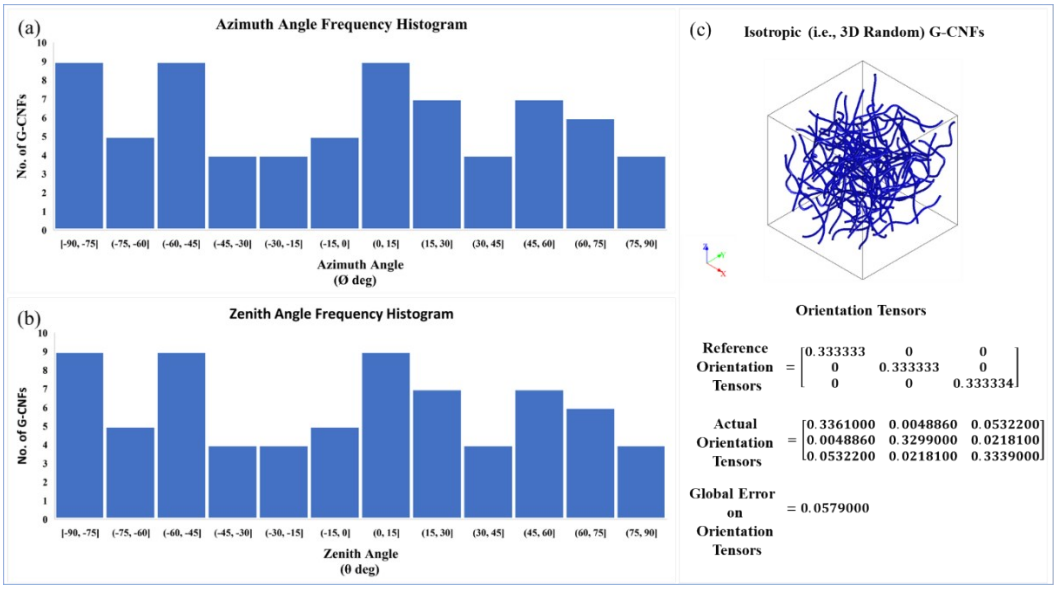

Figure S4 Analysis of the random orientation of the 3D RVE of the G/CNFs Microstructure. (a) Analysis of the distribution of the orientation of the inclusions when measured to Azimuth angle and (b) Zenith angle. (c) Orientation Tensor with the global error.

S2.6 References

1. X. Jin, A. Al-Qatatsheh, K. Subhani and N. V Salim, *Chem. Eng. J.*, 2021, DOI: https://doi.org/10.1016/j.cej.2021.128635, 128635.
2. N. O. Weiss, H. Zhou, L. Liao, Y. Liu, S. Jiang, Y. Huang and X. Duan, *Adv. Mater.*, 2012, **24**, 5782-5825.
3. F. Agend, N. Naderi and R. Fareghi-Alamdari, *J. Appl. Polym. Sci.*, 2007, **106**, 255-259.
4. E. Seran, M. Godefroy, E. Pili, N. Michielsen and S. Bondiguel, *Earth Space Sci.*, 2017, **4**, 91-106.
5. J. D. Eshelby, *Proceedings of the royal society of London. Series A. Mathematical and physical sciences*, 1957, **241**, 376-396.

6. J. D. Eshelby, *Proceedings of the Royal Society of London. Series A. Mathematical and Physical Sciences*, 1959, **252**, 561-569.

7. T. Mori and K. Tanaka, *Acta metall.*, 1973, **21**, 571-574.

8. R. Rodríguez-Ramos, C. Gandarilla-Pérez, L. Lau-Alfonso, F. Lebon, F. Sabina and I. Sevostianov, *Acta Mech.*, 2019, **230**, 3613-3632.

9. W. Ogierman and G. Kokot, *J. Achiev. Mater. Manufac. Eng.*, 2013, **61**, 343-348.

10. S. Sasidharan and A. Anand, *Ind. Eng. Chem. Res.*, 2020, **59**, 12617-12631.

11. O. Pierard, C. Friebel and I. Doghri, *Compos. Sci. Technol.*, 2004, **64**, 1587-1603.

12. Y. Yang, G. Song and Y. Chen, *J. Reinf. Plast. Comp.*, 2015, **34**, 307-314.

13. L. Feng, N. Xie and J. Zhong, *Materials*, 2014, **7**, 3919-3945.

14. I. Gitman, H. Askes and L. Sluys, *Eng. Fract. Mech.*, 2007, **74**, 2518-2534.

15. N. Khani, M. Yildiz and B. Koc, *Mater. Design*, 2016, **109**, 123-132.